Journal of Biomolecular NMR **29:** 243–257, 2004.

Model-free analysis of protein dynamics: assessment of accuracy and model selection protocols based on molecular dynamics simulation

Jianhan Chen, Charles L. Brooks, III & Peter E. Wright
Department of Molecular Biology, The Scripps Research Institute, 10550 North Torrey Pines Road, La Jolla, CA 92037, USA

Received 10 July 2003; Accepted 3 December 2003

Key words: AIC, BIC, hypothesis testing, model selection, NMR relaxation

Abstract

The popular model-free approach to analyze NMR relaxation measurements has been examined using artificial amide ^{15}N relaxation data sets generated from a 10 nanosecond molecular dynamics trajectory of a dihydrofolate reductase ternary complex in explicit water. With access to a detailed picture of the underlying internal motions, the efficacy of model-free analysis and impact of model selection protocols on the interpretation of NMR data can be studied. In the limit of uncorrelated global tumbling and internal motions, fitting the relaxation data to the model-free models can recover a significant amount of quantitative information on the internal dynamics. Despite a slight overestimation, the generalized order parameter is quite accurately determined. However, the model-free analysis appears to be insensitive to the presence of nanosecond time scale motions with relatively small magnitude. For such cases, the effective correlation time can be significantly underestimated. As a result, proteins appear to be more rigid than they really are. The model selection protocols have a major impact on the information one can reliably obtain. The commonly employed protocol based on step-up hypothesis testing has severe drawbacks of oversimplification and underfitting. The consequences are that the order parameter is more severely overestimated and the correlation time more severely underestimated. Instead, model selection based on Bayesian Information Criteria (BIC), recently introduced to the model-free analysis by d'Auvergne and Gooley (2003), provides a better balance between bias and variance. More appropriate models can be selected, leading to improved estimate of both the order parameter and correlation time. In addition, the computational cost is significantly reduced and subjective parameters such as the significance level are unnecessary.

Abbreviations: MD – Molecular Dynamics; NMR – Nuclear Magnetic Resonance; DHFR – *Escherichia coli* dihydrofolate reducase; T_1 – longitudinal relaxation time constant; T_2 – transverse relaxation time constant; NOE – Nuclear Overhauser Effect; AIC – Akaike's Information Criteria; BIC – Bayesian Information Criteria; CSA – Chemical Shift Anisotropy.

Introduction

It is generally believed that the internal dynamics of proteins play an important role in their biological function (Brooks et al., 1988; Ishima and Torchia, 2000). Nuclear Magnetic Resonance (NMR) spectroscopy is one of the most powerful experimental techniques for characterization of protein dynamics (Osorne et al., 2001). Motions over a large range of time scales can be probed at an atomic level. In particular, information about fast atomic motions on picosecond to nanosecond (ps-ns) time scale is encoded in the much slower relaxation processes of nuclear spins. In standard NMR relaxation experiments three relaxation constants, R_1, R_2 and NOE, are measured at many sites along the backbone and in the side chains using isotopically labeled proteins, sometimes, at multiple magnetic fields. Site specific information about the

*To whom correspondence should be addressed. E-mails: brooks@scripps.edu; wright@scripps.edu

amplitude and time scale of internal motions can be derived from these measurements and provide important insights into protein function (Lipari and Szabo, 1982; Palmer, 2001). In turn, thermodynamic parameters which might reflect the change of conformational entropy upon binding can be also estimated (Yang and Kay, 1996; Wrabl et al., 2000; Wand, 2001). Unfortunately, the understanding of internal dynamics of proteins has been hampered by ambiguities in interpreting the relaxation data. Due to the limited number of measurements, intrinsically complex internal motions have to be approximated by simple models with only a few parameters. Assuming that the global and internal motions are separable, the widely used model-free formalism (Lipari and Szabo, 1982; Clore et al., 1990) characterizes internal dynamics in terms of generalized order parameters and time constants, which are motional model independent measurements of the degree of spatial restriction and rate of internal motions respectively. However, how well these simplified models can capture the essential features of protein dynamics is not clear. Additional complications also arise from ambiguities in selecting the best model-free models to fit the experimental data.

Another important tool for studying protein dynamics is molecular dynamics (MD) simulations (Brooks et al., 1988). MD simulations of proteins have become increasingly important and useful, partially due to the development of more realistic force fields and access to ever increasing computational power (Karplus and McCammon, 2002). Actually, it has always played an important role in interpreting biomolecular NMR experimental data (Levy et al., 1981; Brunger et al., 1998; Case, 2002; Prompers and Brüschweiler, 2002). MD is particularly powerful in simulating the ps/ns time scale motions that are relevant to NMR relaxation and provides an effective approach to evaluate various methods for analyzing NMR relaxation data. In the present study, we utilize information from nanosecond MD simulations of a protein complex and try to address the following questions. First, in the limit of uncoupled global molecular tumbling and local diffusion, how much information about the internal dynamics of proteins can be accurately recovered from the model-free analysis? Second, what is the optimal protocol for model selection and what are the impacts of model selection protocols on the results of model-free analysis? By constructing artificial backbone amide ^{15}N relaxation data from long MD trajectories, a detailed picture of the underlying internal motions is accessible. It is thus possible to address these questions in an unambiguous way.

Theory and methods

NMR relaxation theory

Experimental methods have been developed for the measurement of R_1, R_2 and the heteronuclear NOE of amide ^{15}N in protein backbone and side chains (Palmer, 2001). The theory of NMR relaxation has been extensively described (Abragam, 1961; Lipari and Szabo, 1982; Brüschweiler et al., 1992; Cavanagh et al., 1996) and is only summarized here. When cross-correlation effects are suppressed, the amide ^{15}N nuclear spin relaxes primarily due to dipolar interaction with the directly attached ^{1}H spin and through ^{15}N Chemical Shift Anisotropy (CSA). The relaxation constants are determined by the spectral density functions, $J(\omega)$, according to,

$$R_1 = \frac{d^2}{4}[3J(\omega_N) + J(\omega_H - \omega_N) + 6J(\omega_H + \omega_N)] + \frac{c^2}{3}J(\omega_N), \quad (1)$$

$$R_2 = \frac{d^2}{8}[4J(0) + 3J(\omega_N) + J(\omega_H - \omega_N) + 6J(\omega_H) + 6J(\omega_H + \omega_N)] + \frac{c^2}{18}[4J(0) + 3J(\omega_N)] + R_{ex}, \quad (2)$$

$$\mathrm{NOE} = 1 + \frac{d^2}{4R_1}\frac{\gamma_H}{\gamma_N}[6J(\omega_H + \omega_N) - J(\omega_H - \omega_N)], \quad (3)$$

where $d = (\mu_0 h \gamma_H \gamma_N / 8\pi^2) < r_{NH}^{-3} >$ and $c = \Delta\sigma\omega_N$; μ_0 is the permeability of free space; h is Planck's constant; γ_H and γ_N are the gyromagnetic ratios of ^{1}H and ^{15}N; r_{NH} is the length of the N-H bond; $\Delta\sigma$ is the CSA of ^{15}N; ω_H and ω_N are the Larmor frequencies of ^{1}H and ^{15}N. R_{ex} is introduced to account for other processes that contribute to R_2. Usually a non-zero R_{ex} implies the presence of motions on the microsecond to millisecond time scale. The CSA tensor is assumed to be axially symmetric with a principal axis which is co-linear to the N-H bond vector. For typical magnetic fields available at present, ω_N and ω_H range from 50 MHz up to 900 MHz. Thus, NMR relaxation is particularly sensitive to motions on ps/ns time scales.

The spectral density function is the Fourier transform of the angular auto-correlation function, $C(t)$, of the N-H bond vector,

$$J(\omega) = 2\int_0^\infty C(t)\,\cos\omega t\,dt\,. \quad (4)$$

The correlation function describes reorientation of the N-H bond vector due to both the overall molecular tumbling and internal dynamics. Assuming that the overall molecular tumbling is much slower than the internal motions, one can decompose $C(t)$ as (Wallach, 1967)

$$C(t) = C_{\rm O}(t)\,C_{\rm I}(t)\,, \quad (5)$$

where $C_{\rm O}(t)$ and $C_{\rm I}(t)$ are the correlation functions for the overall tumbling and internal motions respectively. When the molecular tumbling is isotropic, the overall motion can be described by a single correlation time, $\tau_{\rm M}^{-1} = 6D_{\rm M}$, i.e.,

$$C_{\rm O}^{\rm iso}(t) = \frac{1}{5}e^{-t/\tau_{\rm M}}\,, \quad (6)$$

where D_M is the isotropic rotational diffusion constant. For the more general case of axially symmetric rotational diffusion, the overall correlation function can be represented by (Woessner, 1962)

$$C_{\rm O}^{\rm axial}(t) = \frac{1}{5}(A_1e^{-t/\tau_1} + A_2e^{-t/\tau_2} + A_3e^{-t/\tau_3})\,, \quad (7)$$

with $A_1 = (1.5\cos^2\alpha - 0.5)^2$, $A_2 = 3\sin^2\alpha\,\cos^2\alpha$, and $A_3 = 0.75\sin^4\alpha$, where α is the angle between the N-H bond vector and principal axis of the rotational diffusion tensor. The diffusional correlation times are $\tau_1^{-1} = 6D_\perp$, $\tau_2^{-1} = D_\parallel + 5D_\perp$, and $\tau_3^{-1} = 4D_\parallel + 2D_\perp$, where $D_\perp = D_x = D_y$, and $D_z = D_\parallel$, with D_x, D_y and D_z being the diagonal elements of the rotational diffusion tensor. The internal correlation function is given as

$$C_{\rm I}(t) = < P_2(\hat{\mu}(0)\cdot\hat{\mu}(t)) >\,, \quad (8)$$

where the second Legendre polynomial $P_2(x) = (3x^2 - 1)/2$, and the unit vector $\hat{\mu}$ describes the orientation of the N-H bond vector in the molecular reference frame.

Model-free analysis

As shown in Equations 1–3, the relaxation constants are determined by the spectral densities at five characteristic frequencies. With the limit of three relaxation measurements at each magnetic field, all five values cannot be determined. In such cases, a reduced spectral density mapping (Peng and Wagner, 1992; Farrow et al., 1995) can be used. However, the more popular approach is to use the so-called model-free formalism (Lipari and Szabo, 1982; Clore et al., 1990). The unknown spectral density function, or equivalently, the internal correlation function, is modeled by simple analytical functions that depend on a few 'model-free' parameters. For example, the internal dynamics can be simply characterized by two motional parameters,

$$C_{\rm I}(t) = \mathbf{S}^2 + (1 - \mathbf{S}^2)\,e^{-t/\tau_e}\,, \quad (9)$$

in which the squared generalized order parameter, $\mathbf{S}^2 = C_{\rm I}(\infty)$, reflects the amplitude of the internal motions and the time constant, τ_e, in this case, equals to the integrated correlation time, $\tau_{\rm eff}$, defined as

$$\tau_{\rm eff} = \frac{1}{C_{\rm I}(0) - C_{\rm I}(\infty)}\int_0^\infty (C_{\rm I}(t) - C_{\rm I}(\infty))\,dt\,. \quad (10)$$

For residues that display more complex internal dynamics, an extended formalism can be used,

$$C_{\rm I}(t) = \mathbf{S}^2 + (1 - \mathbf{S}_f^2)\,e^{-t/\tau_f} + (\mathbf{S}_f^2 - \mathbf{S}^2)\,e^{-t/\tau_s} \quad (11)$$

where τ_f and τ_s are two independent time constants for the fast (ps) and slow (ns) internal motions respectively, $\mathbf{S}_f^2$ and $\mathbf{S}^2$ are the corresponding squared generalized order parameters and $\mathbf{S}^2 = \mathbf{S}_f^2\,\mathbf{S}_s^2$.

Typically, the model-free parameters, i.e., the order parameters and time constants of internal motions, are determined by nonlinear minimization of χ^2 (Palmer et al., 1991),

$$\chi^2 = \sum_{j=1}^{M}(R_j - \hat{R}_j)^2/\sigma_j^2\,, \quad (12)$$

where R_j is the experimental value of the relaxation constant, $\hat{R}_j$ is the corresponding theoretical value, σ_j is the uncertainty of jth relaxation constant, and M is the total number of relaxation measurements. Usually $M = 3$ and $R_j = \{R_1, R_2, \text{NOE}\}$ when the relaxation data are collected at a single magnetic field. The theoretical value $\hat{R}_j$ is back-calculated for given model-free parameters using Equations (1–3). A good estimation of the molecular rotational diffusion tensor, especially the degree of anisotropy, is essential for proper interpretation of the relaxation data. Several methods have been proposed and they generally work well for good quality data sets (Kroenke et al., 1998; Pawley et al., 2001; Osborne and Wright, 2001).

Equation 11 is a more general formalism for describing the internal motions and thus often provides a

better fit to the relaxation data (Tjandra et al., 1995). However, the data might be over fit and the presence of random noise in the experimental data not properly accounted for. In practice, an optimal functional form, i.e., model, needs to be selected to fit the data for each residue. Five models with various combinations of model-free parameters are commonly used in the model-free analysis. They are model 1 $\{\mathbf{S}^2\}$, model 2 $\{\mathbf{S}^2, \tau_e\}$, model 3 $\{\mathbf{S}^2, R_{\rm ex}\}$, model 4 $\{\mathbf{S}^2, \tau_e, R_{\rm ex}\}$ and model 5 $\{\mathbf{S}_f^2, \mathbf{S}_s^2, \tau_s\}$. In models 1, 3 and 5, $\tau_f \rightarrow 0$ is assumed. $R_{\rm ex}$ is assumed to be negligible when absent. In models 1-4, motions on the nanosecond time scale are assumed to be negligible, i.e., $\mathbf{S}_s^2 = 1$. The relaxation data are fit to each model. An optimal model is then selected based on the fitting results.

Model selection theory and implementation

Model selection is an important topic in statistics and has been studied extensively in various contexts (Akaike, 1974; Wax and Ziskind, 1989; Burnham and Anderson, 1998). For example, one of the critical problems in linear prediction is the correct estimation of the number of sinusoids present in the time domain signals (Koehl, 1999). For the application of model-free analysis, the dominant protocol currently in use is based on step-up hypothesis testing using χ^2 statistics and F-tests (Mandel et al., 1995). While it greatly reduces arbitrariness in model selection, this protocol still has several limitations. First, subjective judgment is required in deciding on the significance levels for the tests. Different choices lead to inconsistent model selections. In addition, the model selection also depends on whether step-up or step-down testing is used. Second, only nested models can be tested. It is not possible to compare all five models simultaneously. Ambiguous selection can occur, for example, when both models 2 and 3 are favorable in F-tests. Third, F-tests are not applicable when the number of fitting parameters in any of the models equals to the number of inputs. Last, expensive Monte Carlo simulations are required in order to estimate the χ^2 and F-distributions necessary for hypothesis testing.

Alternatively, another class of protocols, recently introduced to model-free analysis by d'Auvergne and Gooley (2003), is based on frequentist techniques. The idea is to achieve the best balance between bias (oversimplification) and variance (incorporation of experimental noise) by identifying the models that yields the smallest expected discrepancy. A discrepancy can be any measure of lack of fit and the expected discrepancy is the average value of the discrepancy between the true data set and result of fitting to a sample set. Since in practice the true set is not available, the expected discrepancy can never be calculated. Instead, an estimation can be made using the sample data set. Such an estimation is called a 'criterion'. Among various information theoretic criteria, Akaike's Information Criterion (AIC) (Akaike, 1974) and Bayesian Information Criterion (BIC) (Schwarz, 1978) are the simplest and have been shown to provide appropriate model selections for the model-free analysis using some synthetic relaxation data sets generated from some general three-dimensional grids of $\{\mathbf{S}^2, \tau_e, R_{\rm ex}\}$ and $\{\mathbf{S}_f^2, \mathbf{S}_s^2, R_{\rm ex}\}$ (d'Auvergne and Gooley, 2003). Using the definition of empirical Kullback–Leibler discrepancy (Kullback and Leibler, 1951), AIC and BIC are simply given as

$$AIC = \chi^2 + 2k\,, \tag{13}$$

$$BIC = \chi^2 + k \ln M\,, \tag{14}$$

where k is the number of independent parameters in the model and M is the dimension of the sample data set, i.e., the number of independent relaxation measurements. Additional description of related information theory can be found in Burnham and Anderson (1998). Using AIC and BIC, all five models are compared simultaneously and expensive Monte Carlo simulations are totally unnecessary for making a selection. Note that a graphical approach based on Bayesian statistics was also proposed recently by Levy and coworkers (Jin et al., 1998; Andrec et al.,

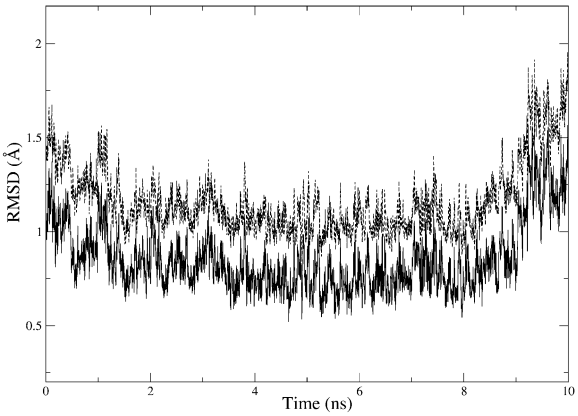

Figure 1. Time dependence of the RMSD between snapshots and the average structure from the 10 ns trajectory of the DHFR/THF/NADPH ternary complex in explicit water. The bottom trace was computed by including only backbone atoms (C_α, C, O and N) and the top trace by including all heavy atoms.

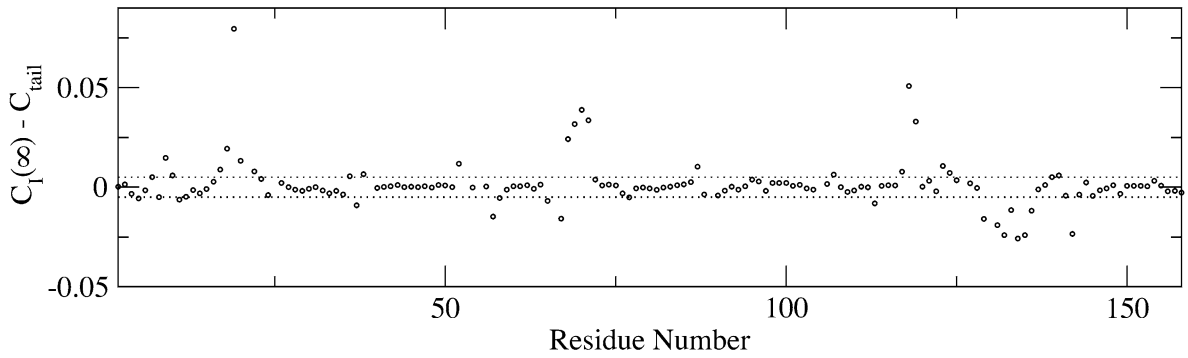

Figure 2. Difference between $C_I(\infty)$, estimated by Equation (16), and C_{tail}, the average of the last 0.5 ns of the internal correlation function. The full length of the correlation functions is $t_{max} = 3$ ns. The difference is very small (between $\pm$ 0.005, indicated by the dotted lines) for most residues, indicating convergence. However, significant differences are observed for some residues.

1999, 2000). However, its practical implementation for model-selection is not yet realized.

The model selection via hypothesis testing was implemented following the flow diagram in (Mandel et al. (1995) with small modifications: when both models 2 and 3 are favorable in F-tests, the one with smaller χ^2 is selected; when neither model 2 nor 3 is selected, models 4 and 5 are considered (never go back to model 1). The acceptance rule for models 4 and 5 is as follows: if $M = 3$, model 4 or 5 is accepted only if $\chi^2 \leq \delta$, with δ being a small number; if $M > 3$, model 4 or 5 is accepted as long as $\chi^2 \leq \chi^2(\alpha')$, where α' is an empirically chosen critical value. If both models 4 and 5 satisfy the acceptance rule, the one with lower χ^2 is selected; if neither is accepted, it is decided that no model sufficiently fits the data and the one with smaller χ^2 is chosen as the best model. Note that F-tests are possible between models 4 & 2, 4 & 3, and 5 & 2 when $M > 3$, however, they are not commonly used. Also note that even though this protocol is not purely based on hypothesis testing, we will still refer to it as the hypothesis testing model selection in the following discussions.

Implementation of AIC and BIC for model selection is straightforward. The model with the smallest criterion is selected as the best model. As neither AIC nor BIC provides any information on the quality of fit to the best model, except what can be induced from χ^2 of fit, additional Monte Carlo simulations are used to determine whether the selected model can sufficiently describe the data. For models 1, 2 and 3, the fit is considered to be sufficient only if $\chi^2 \leq \chi^2(\alpha = 0.1)$, with α being an empirically chosen critical value. For models 4 and 5, the acceptance rules used in the hypothesis testing model selection (see above) are used to determine the quality of the fit. If the selected model does not sufficiently describe the data, it is decided that none of the models can sufficiently fit the data and no effort is attempted on selecting an alternative model. Note that the Monte Carlo simulation step is not part of the AIC or BIC model selection, but an additional check of fit quality for practical purposes.

MD simulation

To explore the accuracy of motional parameters obtained from the model-free analysis and their consistency with the underlying dynamics, we utilized a 10 ns MD trajectory of the DHFR/DHF/NADPH ternary protein complex in explicit water generated using the CHARMM program (Brooks et al., 1983). Dihydrofolate reductase (DHFR) catalyzes the reduction of dihydrofolate (DHF) to tetrahydrofolate (THF) with the cofactor NADPH. Previous MD and NMR studies (Radkiewicz and Brooks, 2000; Osborne et al., 2001) have shown that rich, diverse internal dynamics exists at multiple time scales and this is believed to have significant consequences in the catalytic function of DHFR. Since the MD protocol has been given in detail in Radkiewicz and Brooks (2000), we only briefly describe the simulation methodology here. The protein was characterized by the CHARMM param22 parameter set (MacKerell, Jr. et al., 1998), the water by the TIP3P model (Joregensen et al., 1983), NADPH by a force field developed by Pavelites et al. (1997), and DHF by a force field constructed by Radkiewicz and Brooks (2000). A van der Waals switching function between 8 and 11 Å and an electrostatic shifting function were used. The SHAKE algorithm (Ryckaert et al., 1977) was applied and a time step of 0.002 ps

was used. The coordinates were sampled every 200 steps and a total number of 25,000 snapshots were collected. The stability of the trajectory has been accessed by studying the time evolution of root-mean-square deviation (RMSD) from the X-Ray structure, side chain contacts and hydrogen bonding patterns. It was found that the core structure of the protein complex remained very close to the initial X-Ray structure, while flexible loops were allowed to change conformation.

Data analysis

The key step to calculating the relaxation constants, R_1, R_2 and NOE, from a MD trajectory is computing the angular auto-correlation function of internal motions for each N-H bond vector. Each snapshot was first superimposed onto the average structure of the whole trajectory by a least-squares fit of the protein backbone atoms. The overall molecular tumbling was thus removed and coordinates in the same molecular reference frame resulted. Figure 1 shows the backbone and heavy atom RMSD values from the average structure as a function of time. The internal correlation functions of backbone N-H vectors were then computed using Equation 8. Note that fluctuations in the internuclear separation were not included because the length of all hydrogen-heavy atom bonds was fixed by SHAKE throughout the simulation. It has been shown previously that the effect of SHAKE on simulated order parameters is negligible (Pfeiffer et al., 2001).

Due to the finite length of the MD trajectory, the spectral densities cannot be computed directly using Equation (4). Instead, the internal correlation function is partitioned into 'fast' and 'slow' parts (Brüschweiler et al., 1992). Only the fast part is explicitly computed and the slow part is approximated by a plateau value:

$$J(\omega) \approx 2\int_0^{t_{\max}} C_{\mathrm{I}}(t)C_{\mathrm{O}}(t)\cos(\omega t)\,dt + 2\int_{t_{\max}}^{\infty} C_{\mathrm{I}}(\infty)C_{\mathrm{O}}(t)\cos(\omega t)\,dt\,, \qquad (15)$$

where $t_{\max}$ is the maximum length of explicitly computed correlation function. When the correlation function reaches a plateau value, $C_{\mathrm{I}}(\infty)$ can be estimated from the equilibrium orientational distribution of the dynamics trajectory (Levy et al., 1981; Brüschweiler et al., 1992):

$$C_{\mathrm{I}}(\infty) = \frac{4\pi}{5}\sum_{m=-2}^{2} |\langle Y_{2m}(\theta,\phi)\rangle|^2\,, \qquad (16)$$

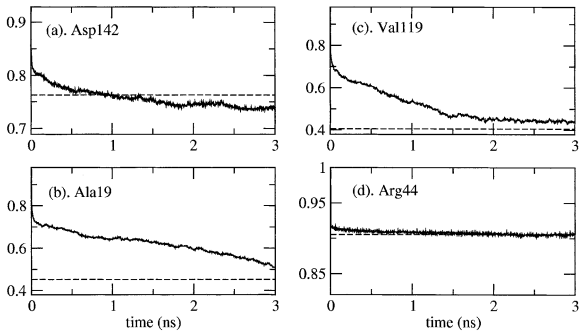

Figure 3. Internal angular autocorrelation functions of backbone N-H vectors for residues (a) Asp142, (b) Ala19, (c) Val119 and (d) Arg44. The broken lines indicate the values of $C_{\mathrm{I}}(\infty)$ given by Equation 16. While (d) is representative of most residues, (a)-(c) are examples of unconverged correlation functions. Note that Ala19 has the largest difference between $C_{\mathrm{I}}(\infty)$ and C_{tail} among all residues.

with (θ, ϕ) being the polar angles of the N-H bond orientation vector $\hat{\mu}$. However, for residues with significant motions on the nanosecond time scale, a plateau value might not be reached by $t_{\max}$. As a result, the correlation function might be discontinuous at $t_{\max}$ in Equation 15, which introduces undesirable artifacts in the spectral density function. This issue will be discussed in more detail in the results section.

The overall tumbling was assumed to be axially symmetric with $\tau_m = 1/(4D_\perp + 2D_\parallel) = 9$ ns and $D_{\mathrm{ratio}} = D_\parallel/D_\perp = 1.2$. The ^{15}N CSA was set to be $\Delta\sigma = -170$ ppm. These values are similar to the experimental results (Osborne and Wright, 2001). Once the spectral densities at five frequencies are available, the relaxation constants can be computed using Equations 1–3. The NMR analysis module in CHARMM (Brüschweiler et al., 1992) was used with minor modifications. The contributions of microsecond/millisecond time scale motions to R_2 were added afterwards using the results of analyzing an experimental data set acquired on a similar complex (Osborne and Wright, 2001). The R_{ex} terms were assumed to scale quadratically with respect to the strength of magnetic field.

Fitting of the relaxation data to model-free models was carried out using the ModelFree 4.15 software package (Palmer et al., 1991; Mandel et al., 1995). The same values of τ_m, D_{ratio} and CSA were used in all analysis. The N-H bond length was set to be 0.997Å instead of the common value of 1.02Å to be consistent with the equilibrium N-H bond length of the dynamics trajectory. Grid search was always used before χ^2 minimization. Twenty increments were used

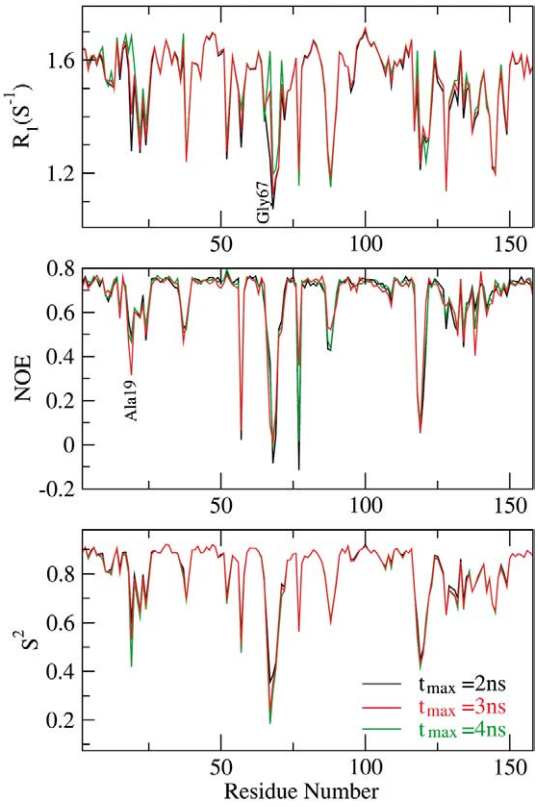

Figure 4. Values of R_1, NOE and $\mathbf{S}^2$ at 500 MHz with $t_{\max} = 2$, 3 and 4 ns. Except for a few residues such as Ala19 and Gly67, the relaxation constants only differ slightly with respect to $t_{\max}$. $\mathbf{S}^2$ is first estimated as $C_{\mathrm{I}}(\infty)$, then shifted to C_{tail} if $|C_{\mathrm{I}}(\infty) - C_{\mathrm{tail}}| > 0.005$, where C_{tail} is average of the last one sixth of the correlation function.

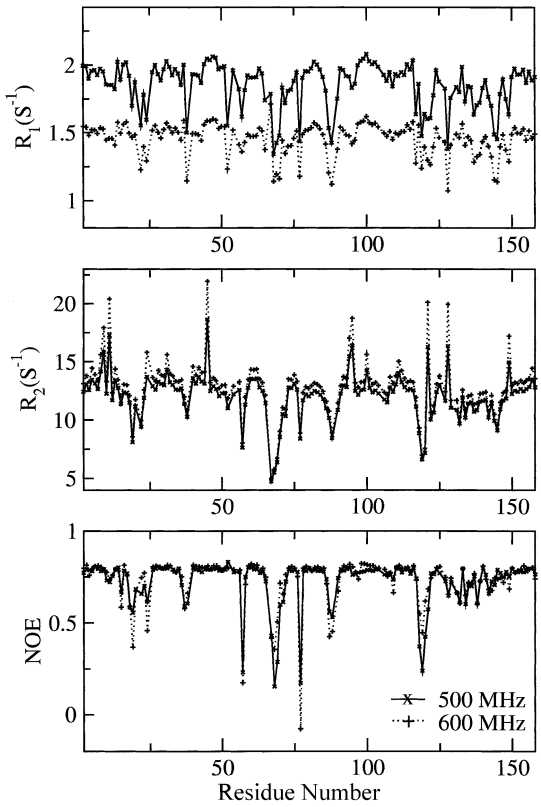

Figure 5. Simulated relaxation constants extracted from a 10 ns dynamics trajectory with $t_{\max} = 3$ ns at two magnetic fields that correspond to proton Larmor frequencies of 500 and 600 MHz respectively.

in the grid search for each parameter except that fifty increments were used for τ_s in model 5. The purpose of a finer grid is to avoid potential failure of the nonlinear minimization due to a larger dynamic range. The search ranges were set to be between 0 and 1 for the order parameters, 0 and 10 s^{-1} for R_{ex}, 0 and 1000 ps for τ_e in models 2 and 4, and 0 and 4500 ps for τ_s in model 5. All Monte Carlo simulations were performed with ModelFree 4.15 option 'sim_type' set to 'pred'.

Results and discussion

Convergence of simulated relaxation data

As discussed previously, due to the finite length of the MD trajectory, the autocorrelation function is only explicitly computed up to a maximum time $t_{\max}$ and Equation 15 has to be used to construct the spectral density functions. This partitioning of the correlation function is a good approximation to the exact definition of Equation 4 for most residues. As shown in Figure 2, the difference between $C_{\mathrm{I}}(\infty)$, computed from Equation 16, and C_{tail}, the average of the last 0.5 ns of the correlation function, is very small (< 0.005) for most residues, indicating convergence. However, for some residues, typically those which display significant motions on the nanosecond time scale, the internal correlation function does not fully decay to a plateau value by $t_{\max}$, leading to a significant difference between $C_{\mathrm{I}}(\infty)$ and C_{tail}. Some examples of the correlation functions are shown together with the corresponding values of $C(\infty)$ in Figure 3. The discontinuity of $C(t)$ at $t_{\max}$ leads to artifacts in the spectral density function, which, in turn, results in inconsistent relaxation constants. While the ultimate solution is running a longer simulation, in the present study, the discontinuity was removed simply by replacing $C_{\mathrm{I}}(\infty)$ with C_{tail} when the difference was

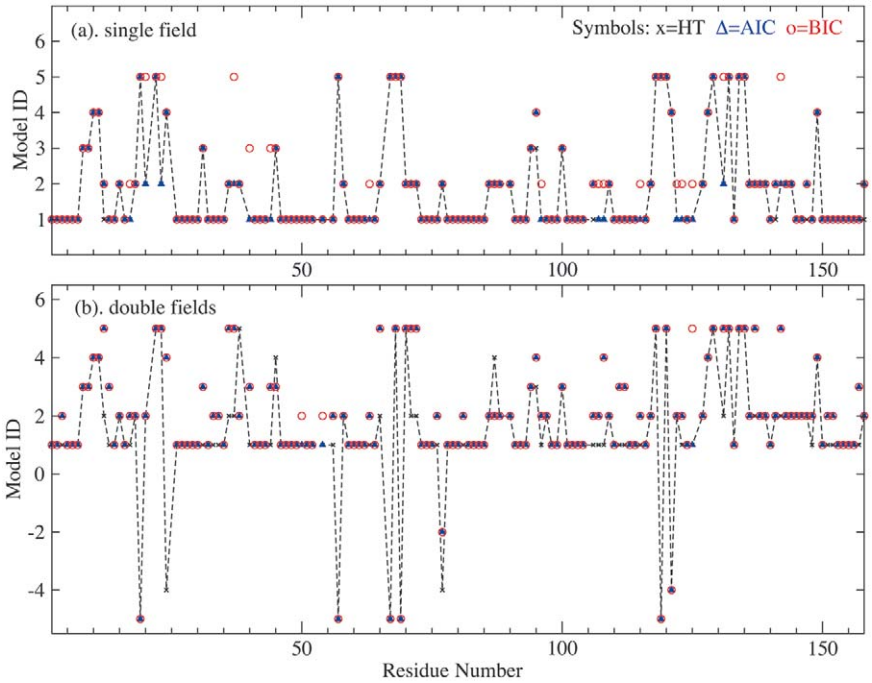

Figure 6. Model selection results using the relaxation data at (a) 500 MHz, and (b) both 500 and 600 MHz. The broken line connects IDs of the models selected by hypothesis testing (HT) for adjacent residues. Blue triangles indicate the models selected by AIC and red circles show those selected by BIC. A negative model ID indicates that the selected model can't sufficiently fit the data.

greater than 0.005. Since the purpose of this study is not to compare the simulated results with experimental values, this approach is justified as long as self-consistency is maintained. Note that we avoid parameterizing the raw correlation functions (e.g., in Pfeiffer et al. (2001)) with the intention of keeping the underlying internal dynamics as realistic as the quality of the simulation allows.

As the correlation function becomes increasingly noisy with longer time, it is necessary to examine the convergence of simulated relaxation constants with respect to t_{max}. The transverse relaxation constant R_2 is mainly determined by the zero frequency component of the spectral density function and converges quickly with respect to t_{max}. R_1 and NOE depend on the high-frequency components and have a stronger dependence on t_{max}. Figure 4 compares values of R_1, NOE and $\mathbf{S}^2$ computed with $t_{max} = 2$, 3 and 4 ns. R_2 values are virtually the same for all three cases and not shown in the figure. Overall convergence is very good except for a few residues such as Ala19 and Gly67. The final relaxation data sets used in the following model-free analysis were generated with $t_{max} = 3$ ns, which are shown in Figure 5. Excluding proline and terminal residues, relaxation constants were computed for a total of 147 backbone amide ^{15}N nuclear spins.

Model-free analysis

Uncertainties in the relaxation constants are necessary to estimate the χ^2- and F-distributions via Monte Carlo simulations. Arbitrary relative uncertainties of 3.0%, 2.5%, and 3.5% were assigned to R_1, R_2 and NOE respectively. In addition, a minimum uncertainty of 0.02 is imposed for NOEs to prevent assigning unrealistically small uncertainties for some residues with very small NOEs. These values are typical for experimental relaxation data sets.

Model selection

Model selection was made following the protocols described in the previous section. Standard critical values of $\alpha = 0.1$ for χ^2 and $\alpha = 0.2$ for F-tests were used in hypothesis testing. $\delta = 0.01$ and $\alpha' = 0.05$ were used in the acceptance rule for models 4 and 5. 200 Monte Carlo simulations were carried out to generate all χ^2- and F-distributions.

The model selection results are summarized in Figure 6 and Table 1. Figure 6a compares the results of model selection by hypothesis testing (denoted HT),

Table 1. Summary of model selection results. The numbers in parenthesis indicate the number of residues for which particular models are selected but then found to insufficiently describe the relaxation data

Data	Protocol	Model 1	Model 2	Model 3	Model 4	Model 5
	HT	93(0)	28(0)	7(0)	6(0)	13(0)
Single	AIC	88(0)	33(0)	6(0)	7(0)	13(0)
Field	BIC	77(0)	37(0)	8(0)	7(0)	18(0)
	HT	85(0)	31(0)	7(0)	7(2)	10(5)
Double	AIC	62(0)	40(1)	12(0)	7(1)	19(5)
Field	BIC	59(0)	42(1)	12(0)	7(1)	20(5)

AIC and BIC when only data at 500 MHz were analyzed. Similar models were selected for most residues by all three protocols and all residues were sufficiently fit by the selected models. AIC selected the same models as HT except for 6 residues (model 2 instead of model 1 for five residues, and model 4 instead of model 3 for one residue), while BIC selected different models for about twenty residues, for which models 2 and 5 were preferred, indicating that BIC is more sensitive in detecting both fast (ps) and slow (ns) internal motions. Examination of the correlation functions shows that these motions are genuine. It is evident that hypothesis testing and AIC selected oversimplified models and caused under-fitting for these residues. These statements will be supported with more detail in the next two sections.

Figure 6b compares the models selected by the three protocols when the relaxation data at both fields were fit together. The selection results are different from those shown in panel (a) in several ways. First, many residues were fit by models of higher complexity for all three protocols. Second, AIC showed a significant improvement in the performance and selected the same models as BIC except for three residues: model 1 was selected for Ile50, Leu54 and Phe125 by AIC, while models 2, 2 and 5 were selected respectively by BIC. The reason is that AIC may perform poorly if the number of parameters is large with respect to the data size (Burnham and Anderson, 1998). On the contrary, HT benefited less from the larger data size and performed poorly compared to AIC and BIC, failing to select the most appropriate models for over 20% of the residues. The problem of over-simplification is more evident. Third, several residues cannot be sufficiently fit by any model. χ^2 for these residues ranges from below 10 to about 100 when fit to the best models, with the largest χ^2 being 93.5 for Ala19. Note that similar models were selected and could sufficiently describe the relaxation data at 500 MHz. Therefore, the availability of additional data does not only help to identify the presence of nanosecond time scale motions for more residues, but also help to reveal the highly complex nature of the underlying dynamics.

In summary, for model selection in the model-free analysis of NMR relaxation data, BIC seems to be the optimal protocol, while AIC performs nearly as well when data is available at two magnetic fields. It is evident that hypothesis testing has severe drawback of selecting oversimplified models. The impacts of different model selections on the motional parameters will be discussed in the next section. In addition, the computational cost of the BIC and AIC model selection is much lower than that of hypothesis testing.

Accuracy of model-free parameters

In this section, we compare the model-free results to the values directly computed from the dynamics trajectory, and discuss the impacts of model selection on the accuracy of the analysis. In order to make direct comparison, the correlation time of nanosecond time scale motions, τ_s, obtained by fitting to model 5 needs to be converted to the effective correlation time defined in Equation 10. Substituting Equation 11 into Equation 10 and assuming $\tau_f \rightarrow 0$, we have

$$\tau_{\text{eff}} = \frac{\mathbf{S}_f^2 - \mathbf{S}^2}{1 - \mathbf{S}^2}\, \tau_s \,. \tag{17}$$

The uncertainty of τ_{eff} was converted from that of τ_s by the same linear relation. The MD values of the effective correlation time were obtained by direct integration of the raw correlation functions according to Equation 10.

When data at a single field were used, AIC and HT selected essentially identical models (see previous section). For clarity, Figure 7 only compares the model-free results obtained with the HT and BIC model selection protocols to the MD values. Among the three motional parameters, the order parameters were reproduced most accurately. As shown in the top panel, the relative errors are below 5% for most residues except for a few in the most flexible regions. On average, the order parameters were over-estimated by about 1.5%. The average absolute error of $\mathbf{S}^2$ is 0.012 ± 0.014 for HT and 0.011 ± 0.013 for BIC, with the maxima both being 0.097 for Gly121. Note that the different, usually more complex, models se-

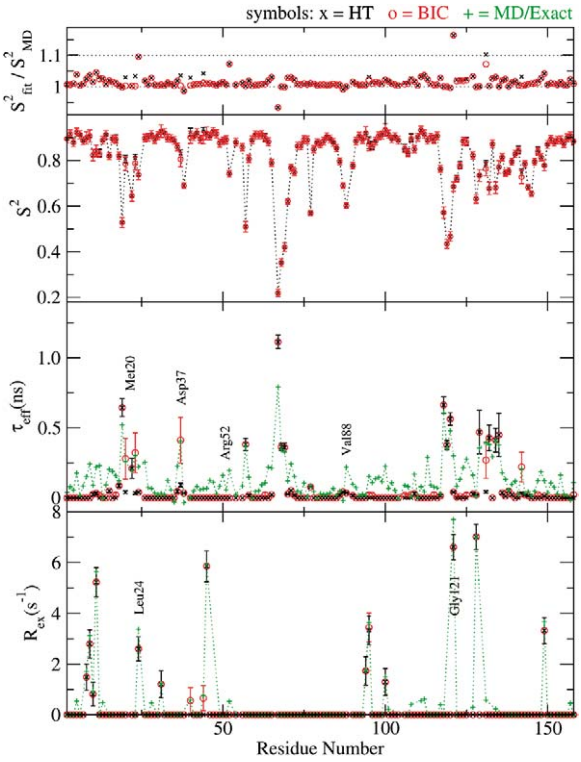

Figure 7. Comparison of model-free parameters obtained by model-free analysis of simulated ^{15}N relaxation data at 500 MHz with corresponding values directly computed from the dynamics trajectory. The results of model-free analysis with HT model selection are shown by black crosses and those with BIC model selection by red circles. The MD/exact values are represented by green pluses. The dotted lines connect the values of parameters obtained with the methods indicated by the colors. Results obtained with AIC model selection are similar to those of using HT model selection and not shown.

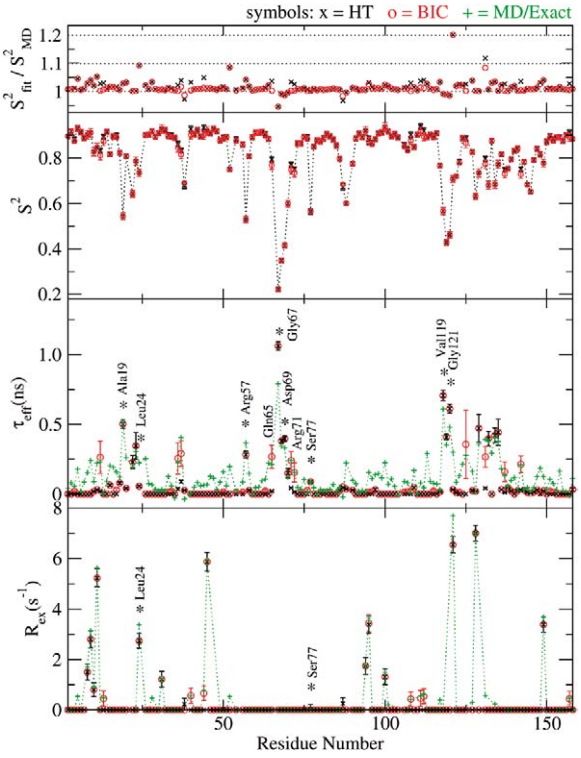

Figure 8. Comparison of model-free parameters from model-free analysis of simulated ^{15}N relaxation data at both 500 and 600 MHz with corresponding values directly computed from the dynamics trajectory. Notations are the same as those in Figure 7. No model sufficiently fit the data for some residues. Results of fitting the data to the best models were shown instead, which are indicated by *'s in τ_{eff} and R_{ex} panels.

lected by BIC all led to more accurate $\mathbf{S}^2$ values. R_{ex} terms were also accurately reproduced. All significant R_{ex} terms were recovered except for a few residues with very small R_{ex}. With the BIC model selection, more small R_{ex} terms were properly identified and no spurious R_{ex} terms occurred. However, this may not be typical when experimental data are to be analyzed. The reason is that inconsistency may exist between the relaxation constants, as they are separate measurements, and would lead to spurious, small R_{ex}, which does not necessarily imply the presence of slow motions on the microsecond to millisecond time scale. The largest deviation between the model-free and MD values was observed in the effective correlation times, τ_{eff}. BIC did a better job in detecting the nanosecond time scale motions than HT and AIC for several residues, such as Met20 and Asp37, which was reflected in more accurate estimates of the effective correlation times. However, τ_{eff} was still significantly underestimated for many residues, especially those with $\tau_{eff} \sim 200$ ps. For some of these residues, such as Leu24 and Gly121, the underestimation can be attributed to the presence of significant R_{ex} contribution and the limit of three parameters per model prevents incorporating τ_s and R_{ex} simultaneously. For others, such as Arg52 and Val88, it seems that motions on the nanosecond time scale have small magnitude and the model-free analysis is insensitive in detecting these motions. The underlying internal dynamics will be examined in more detail in the next section. Note that arbitrarily lowering the uncertainties of the relaxation constants, e.g., to less than 1%, could reveal more nanosecond time scale motions and also lead to more residues that could not be fit by any model (data not shown). However, such small uncertainties are not realistic experimentally.

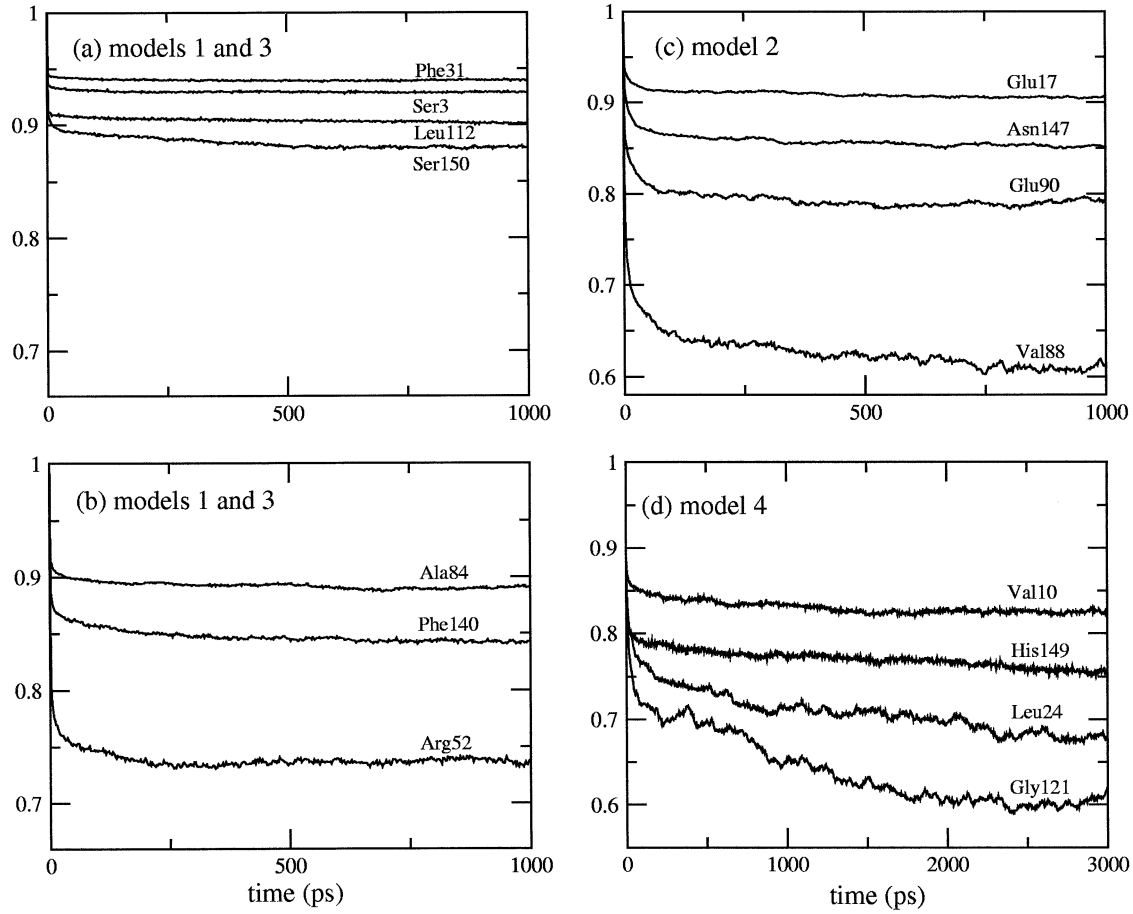

Figure 9. Examples of the internal correlation function for residues that were fit by models 1 to 4. The model selection was made by BIC using data at both fields.

Table 2. Comparison of the average values of motional parameters obtained by model-free analysis (MF) and computed from the dynamics trajectory (MD), categorized by the models. Model selection was made based on BIC using simulated relaxation data at both fields. Results of fitting to the best model were included when no model sufficiently described the relaxation data

Model	τ_{eff} / ps		S^2	
selection	MD	MF	MD	MF
Model 1	79 ± 72	0	0.88 ± 0.03	0.89 ± 0.03
Model 2	95 ± 64	27 ± 17	0.80 ± 0.08	0.81 ± 0.08
Model 3	75 ± 82	0	0.90 ± 0.02	0.91 ± 0.02
Model 4	141 ± 97	27 ± 13	0.75 ± 0.10	0.78 ± 0.08
Model 5	336 ± 150	370 ± 177	0.64 ± 0.16	0.65 ± 0.16

In Figure 8, we examine the results of fitting relaxation data at both fields simultaneously to the model-free models. A summary is given in Table 2. Similar observations can be made, i.e., R_{ex} and S^2 were recovered quite accurately while τ_{eff} was significantly underestimated for many residues. The effective correlation times were more accurately estimated for several residues, such as Gln65 and Arg71, which was a direct consequence of improved ability in detecting nanosecond time scale motions with more data. More small R_{ex} contributions were properly identified by AIC and BIC. There is an obvious reduction in the uncertainties of nonlinear least-squares fitting. However, it is not always associated with an improvement in the accuracy, as compared to the MD values. The underestimation of the fitting uncertainty is probably a consequence of neglecting the ambiguities in the model choice (Andrec et al., 1999). An interesting observation is that for the residues that can not sufficiently described by any model, the motional parameters extracted from fitting to the best models

still reproduce the MD values reasonably well. As discussed previously, similar models were selected by BIC and sufficiently described the data at 500 MHz. This can be considered as an indication of complex underlying internal dynamics. When analyzing experimental data sets, the selected model might fail to provide a sufficient fit simply because of noisy data. It is possible to distinguish these two cases by examining the uncertainties and χ^2 value of the fit. In the current analysis, the error bars of the motional parameters are similar and the residual χ^2 of fit is reasonably small, which can be considered as an indication that the model fails to fit the data because of complex motions. This is also anticipated to be true when analyzing experimental relaxation data sets.

Consistency with underlying dynamics

Consistency of the model-free results with the underlying internal dynamics has also been examined. Examples of the internal correlation functions are shown in Figures 9 and 10. Model selection was made by BIC using relaxation data at both fields. In general, most residues fit by models 1 and 3 do display simple internal dynamics. The corresponding correlation function can be well described by a single exponential that quickly decays to a plateau value. The examples shown in Figure 9a are representative of most residues fit by models 1 and 3. However, the correlation functions of some residues fit by models 1 and 3, such as those shown in Figure 9b, are actually similar to those of residues fit by model 2, shown in Figure 9c. There is not always a distinctive difference in the underlying ps/ns time scale internal dynamics between residues fit by models 1 and 3 and those fit by model 2. As shown in Table 2, the average MD effective correlation time for residues fit with model 2 is only slightly higher than that of residues fit by model 1 and similar to that of residues fit by model 3. Noticeably, some residues fit by models 1-3 do display significant nanosecond time scale motions, such as Arg52 and Val88, with corresponding $\mathbf{S}_s^2$ estimated to be about 0.9 or greater. The model-free analysis seems to be insensitive in detecting nanosecond time scale motions of relatively smaller magnitude; as a result, the effective correlation time is significantly underestimated. For residues with a large R_{ex} contribution, due to the limit of three parameters in the models, nanosecond time scale motions can not be properly identified. As shown in Figure 9, residues fit by model 4 can display significant nanosecond time scale motions. The effective correlation times are most severely underestimated and the order parameter most severely overestimated compared to residues without significant R_{rex} contributions.

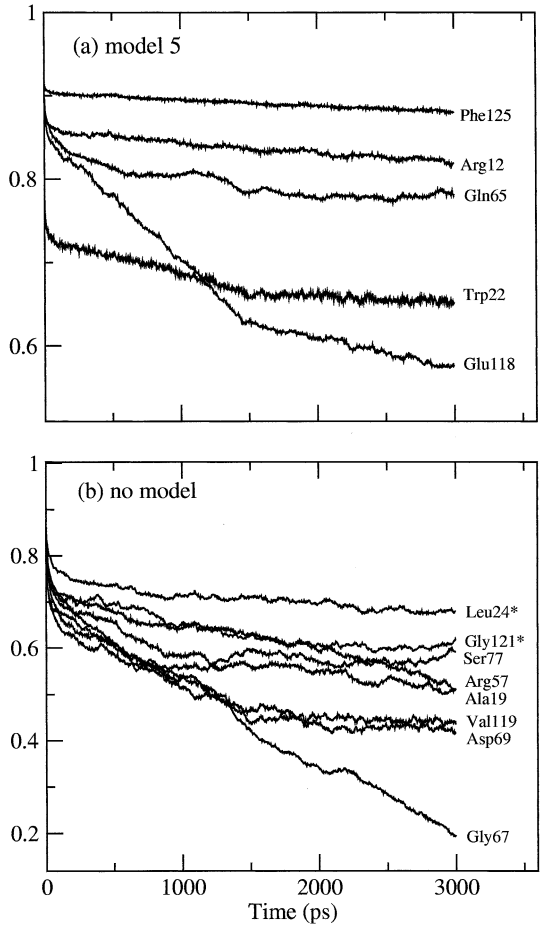

Figure 10. Examples of internal correlation functions for residues sufficiently fit by (a) model 5 and (b) no model. The model selection was made by BIC using simulated relaxation data at both fields. For residues shown in panel (b), the best model is model 4 for Leu24 and Gly121 and model 5 for the rest.

The correlation function of residues that were fit by model 5, shown in Figure 10a, confirms the presence of nanosecond time scale internal motions. The squared order parameter for these motions ranges from below 0.6 to over 0.9. Even though very few correlation functions can be completely described by the functional form of Equation 11, when the presence of nanosecond time scale motions is properly identified, both the order parameter and effective correlation time can be predicted by the model-free analysis quite accurately. This is also true for the residues that could not be sufficiently fit by any model but were best described by model 5. As shown in Table 2, the average values of both the squared order parameters

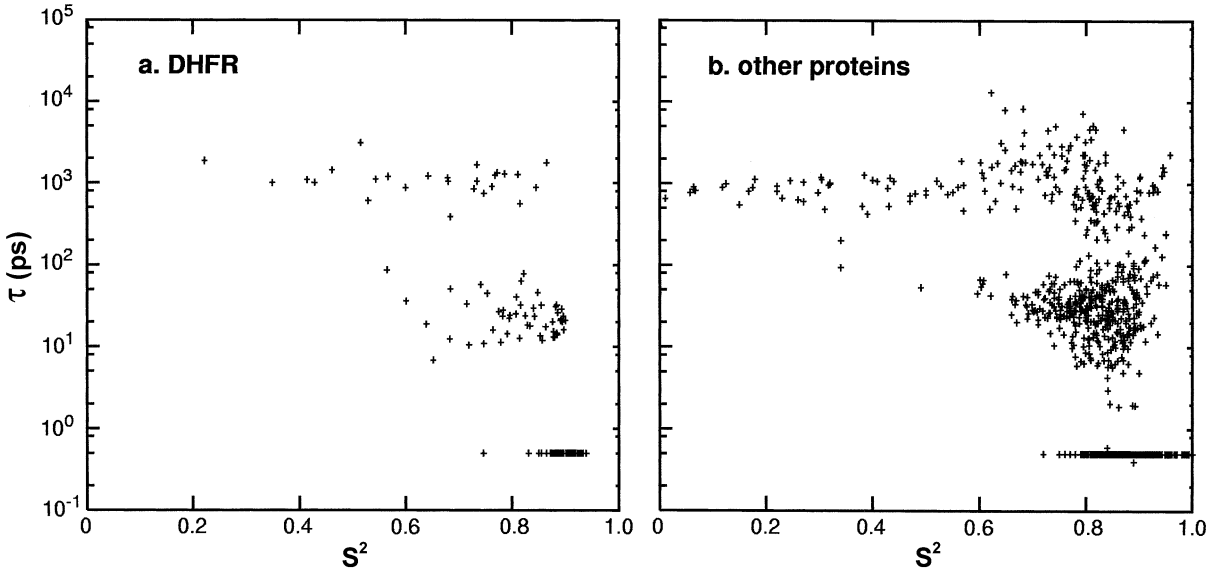

Figure 11. Comparison of the motional parameter space of (a) DHFR and (b) over a dozen of other proteins, which include *E. coli* RNase H (Tugarinov et al., 2001), *E. coli* adenylate kinase (Tugarinov et al., 2002), chemokine eotaxin-3 (Ye et al., 2001), the human – *E. coli* thioredoxin chimera (Dangi et al., 2002), plastocyanin in both oxidation states (Bertini et al., 2001), the TGFβ type II receptor extracellular domain (Deep et al., 2003), four protein inhibitors of serine proteinases (OMTKY3, OMTKY3*, OMIPF3, and OMIPF3*) (Song and Markley, 2003), RNase A (Cole and Loria, 2002), reduced plastocyanin (Ma et al., 2003), reduced and oxidized glutaredoxin (Kelley et al., 1977), and apo calbindin D_{9k} (Akke et al., 1993). All the motional parameters were obtained by model-free analysis of backbone ^{15}N relaxation data, simulated from a 10ns MD trajectory for DHFR and experimentally measured for the rest. The correlation time, τ, was set to τ_s when τ_s was present in the model and τ_f when τ_s was not used in the model. When the data was fit by models 1 and 3, τ was set to 0.5 ps in order to plot on the log-scale y axis.

and effective correlation times obtained by the model-free analysis agree very well with the MD values for residues fit by model 5. Also note that the correlation functions shown in Figure 10b do not necessarily display higher complexity than those of residues fit by model 5, shown in Figure 10a.

Generality of the study

There is an important issue about the generality of the findings described above, as only a single protein has been used. Even though DHFR has been shown to be a very interesting system that displays rich, diverse internal dynamics (Osborne et al., 2001) and is believed to be representative of the internal dynamics commonly seen in other proteins, it is necessary to validate it, for example, by comparing the accessible motional parameter spaces covered by DHFR and other proteins. As the most significant difference observed in the three model selection protocols lies in the ability to detect the presence of nanosecond timescale motions, we examine the $\{\mathbf{S}^2, \tau_e\}$ space accessible to DHFR and over a dozen of other proteins of various sizes and types, for which dynamic data were published recently. As shown in Figure 11, the parameter space accessible to DHFR is quite representative of that of this ensemble of proteins. In addition, only a limited portion of the full parameter space is commonly accessible to proteins. On the contrary, it seems that the general grids used in a previous study (d'Auvergne and Goolley, 2003) do not reflect this limited accessible motional space. This is likely the reason that BIC instead of AIC is found to be the optimal protocol for model selection in model-free analysis. For the same reason, the findings presented in current study seem to be more relevant to model-free analysis of NMR relaxation measurements of proteins.

Conclusions

We have used molecular dynamics simulations to examine the popular model-free approach for analyzing the NMR relaxation measurements. Using a 10 ns explicit solvent dynamics trajectory on a DHFR ternary complex, backbone amide ^{15}N relaxation constants were computed and then analyzed using the model-free approach. By comparing the model-free results

with the values directly computed from the trajectory and by examining the consistency with the underlying internal dynamics, we were able to assess the efficiency of the model-free analysis and study the influence of model selection protocols on the results.

It was found that current protocol of model selection via step-up hypothesis testing is inefficient and suboptimal. Oversimplified models are often selected, which leads to under fitting, as previously shown by d'Auvergne and Gooley (2003). Instead, model selection based on Bayesian Information Criterion (BIC) seems to be an optimal protocol. No subjective parameter such as significance levels is required and all models are compared simultaneously. More appropriate models can be selected and the problem of under fitting is reduced. Akaike's Information Criterion (AIC) also performs well when data is available at two magnetic fields. However, AIC performs almost as poorly as hypothesis testing when data is only available at a single field. Therefore, BIC is preferred for the model selection in the model-free analysis. In additional, the AIC and BIC protocols are computationally more efficient, as Monte Carlo simulations are only necessary for generating χ^2-distributions to determine the quality of the final fit.

In the limit of uncorrelated overall tumbling and internal motions, the model-free analysis seems to be able to provide quantitative information on the internal dynamics. Despite a slight overestimation, the order parameters can be recovered quite accurately. Significant contributions of micro/millisecond motions to the traverse relaxation can also be reliably identified. However, the effective correlation times are often significantly underestimated. Even though BIC greatly reduces the problem of under fitting, the model-free analysis seems to be intrinsically insensitive in detecting the presence of nanosecond time scale motions of relatively small magnitude. Sometimes nanosecond time scale motions with a corresponding squared order parameter as low as 0.9 can go undetected, even with good quality data available at two magnetic fields. Despite the fact that the underlying dynamics is generally more complex than can be described by the model-free models, both the order parameter and effective correlation time can be accurately predicted when the presence of nanosecond time scale motions is properly identified.

A critical assumption of the model-free analysis is that the overall tumbling can be uncoupled from the internal dynamics. This has been expected to be a good approximation for well-folded proteins if the amplitude of internal motions is sufficiently small and the time scale separation between overall tumbling and internal motions is sufficiently large (Case, 2002). Recently, this assumption was called into question (Tugarinov et al., 2001, 2002). By explicitly modeling the coupling between global tumbling and internal motions using the two-body Slowly Relaxing Local Structure (SRLS) theory, dramatic discrepancies with the model-free analysis were reported in both the order parameters and correlation times for several proteins. It is not clear at this point whether the model-free or SRLS analysis provides a more realistic picture of the internal dynamics of proteins. One possible way to address this question is carry out a very long MD simulation, preferably on complex systems with diverse internal motions such as DHFR. This will be addressed in forthcoming publications.

Acknowledgements

CJH thanks a La Jolla Interface of Science postdoctoral fellowship for partial financial support. CJH is deeply grateful to Wonpil Im for significant help and insightful discussions. Jason Schnell, Dan McElheny and Thomas Rod are also acknowledged for helpful discussions. This work was supported by funds from the National Institute of Health (GM56879, PEW and GM48807, CLBIII).

References

Abragam, A. (1961) *The Principles of Nuclear Magnetism*, Clarendon Press, Oxford.

Akaike, H. (1974) *IEEE Trans. Automat. Contr.*, **AC-19**, 716–723.

Akke, M., Skelton, N.J., Kordel, J., Palmer, A.G., III and Chazin, W.J. (1993) *Biochemistry*, **32**, 9832–9844.

Andrec, M., Montelione, G.T., and Levy, R.M. (1999) *J. Magn. Reson.*, **139**, 408–421.

Andrec, M., Montelione, G.T. and Levy, R.M. (2000) *J. Biomol. NMR*, **18**, 83–100.

Bertini, I, Bryant, D.A., Ciurli, S., Dikiy, A., Fernandez, C.O., Luchinat, C., Safarov, N., Vila, A.J. and Zhao, J. (2001) *J. Biol. Chem.*, **276**, 47217–47226.

Brooks, B.R., Bruccoleri, R.E., Olafson, B.D., States, D.J., Swaminathan, S., and Karplus, M. (1983) *J. Comput. Chem.*, **4**, 187–217.

Brooks, III, C.L., Karplus, M. and Pettitt, B.M. (1988) *Proteins: A Theoretical Perspective of Dynamics, Structure, and Thermodynamics*, John Wiley and Sons, New York.

Brunger, A.T., Adams, P.D., Clore, G.M., DeLano, W.L., Gros, P., Grosse-Kunstleve, R.W., Jiang, J.-S., Kuszewski, J., Nilges, N., Pannu, N.S., Read, R.J., Rice, L.M., Simonson, T. and Warren, G.L. (1998) *Acta. Cryst.*, **D54**, 905–921.

Brüschweiler, R., Roux, B., Blackledge, M., Griesinger, C., Karplus, M. and Ernst, R.R. (1992) *J. Am. Chem. Soc.*, **114**, 2289–2302.

Burnham, K.P. and Anderson, D.R. (1998) *Model Selection and Inference: A Practical Information-Theoretic Approach*, Springer-Verlag, New York.

Case, D.A. (2002) *Acc. Chem. Res.*, **35**, 325–331.

Cavanagh, J., Faribrother, W.J., Palmer, III, A.G. and Skelton, M.J. (1996) *Protein NMR Spectroscopy: Principles and Practice*, Academic Press, San Diego.

Clore, G.M., Szabo, A., Bax, A., Kay, L.E., Driscoll, P.C. and Gronenborn, A.M. (1990) *J. Am. Chem. Soc.*, **112**, 4989–4991.

Cole, R. and Loria, J.R. (2002) *Biochemistry*, **41**, 6072–6081.

Dangi, B., Dobrodumov, A.V., Louis, J.M. and Gronenborn, A.M. (2002) *Biochemistry*, **41**, 9376–9388.

d'Auvergne, E.J. and Gooley, P.R. (2003) *J. Biomol. NMR*, **25**, 25–39.

Deep, S., Walker, III, K.P., Shu, Z. and Hinck, A.P. (2003) *Biochemistry*, **42**, 10126–10139

Farrow, N.A., Zhang, O., Szabo, A., Torchia, D.A. and Kay, L.E. (1995) *J. Biomol. NMR*, **6**, 153–162.

Ishima, R. and Torchia, D.A. (2000) *Nat. Struct. Biol.*, **7**, 740–743.

Jin, D., Andrec, M., Montelione, G.T. and Levy, R.M. (1998) *J. Biomol. NMR*, **12**, 471–492.

Joregensen, W.L., Chandrasekhar, J., Madura, J.D., Impey, R.W. and Klein, M.L. (1983) *J. Chem. Phys.*, **79**, 926–35.

Karplus, M. and McCammon, J.A. (2002) *Nat. Struct. Biol.*, **9**, 646–652.

Kelley, III, J.J., Caputo, T.M., Eaton, S.F., Laue, T.M. and Bushweller, J.H. (1997) *Biochemistry*, **36**, 5029–5044.

Koehl, P. (1999) *Prog. NMR. Spec.*, **34**, 257–299.

Kroenke, C.D., Loria, J.P., Lee, L.K., Rance, M. and Palmer, III, A.G. (1998) *J. Am. Chem. Soc.*, **120**, 7905–7915.

Kullback, S. and Leibler, R.A. (1951) *Ann. Math. Stat.*, **22**, 79–86.

Levy, R. M., Karplus, M. and Wolynes, P.G. (1981) *J. Am. Chem. Soc.*, **103**, 5998–6011.

Lipari, G. and Szabo, A. (1982) *J. Am. Chem. Soc.*, **104**, 4546–4559.

Ma, L., Hass, M.A.S., Vierick, N., Kristensen, S.M., Ulstrup, J. and Led, J.J. (2003) *Biochemistry*, **42**, 320–330.

MacKerell, Jr., A.D., Bashford, D., Bellott, M., Dunbrack, R.L., Evanseck, J.D., Field, M.J., Fischer, S., Gao, J., Guo, H., Ha, S., Joseph-McCarthy, D., Kuchnir, L., Kuczera, K., Lau, F.T.K., Mattos, C., Michnick, S., Ngo, T., Nguyen, D.T., Prodhom, B., Reiher, III, W.E., Roux, B., Schlenkrich, M., Smith, J.C., Stote, R., Straub, J., Watanabe, M., Wiorkiewicz-Kuczera, J., Yin, D. and Karplus, M. (1998) *J. Phys. Chem. B*, **102**, 3586–3616.

Mandel, A.M., Akke, M. and Palmer, III, A.G. (1995) *J. Mol. Biol.*, **246**, 144–163.

Osborne, M.J. and Wright, P.E. (2001) *J. Biomol. NMR*, **19**, 209–230.

Osborne, M.J., Schnell, J., Benkovic, S.J., Dyson, H.J. and Wright, P.E. (2001) *Biochemistry*, **40**, 9846–9859.

Palmer, III, A.G. (2001) *Annu. Rev. Biophys. Biomol. Struct.*, **30**,129–155.

Palmer, A.G., Rance, M. and Wright, P.E. (1991) *J. Am. Chem. Soc.*, **113**, 4371–4380.

Pavelites, J.J., Gao, J., Bash, P.A., Alexander, D. and Mackerell, J. (1997) *J. Comput. Chem.*, **18**, 221–229.

Pawley, N.H., Wang, C., Koide, S. and Nicholson, L.K. (2001) *J. Biomol. NMR*, **20**, 149–165.

Peng, J.W. and Wagner, G. (1992) *J. Magn. Reson.*, **98**, 308–332.

Pfeiffer, S., Fushman, D. and Cowburn, D. (2001) *J. Am. Chem. Soc.*, **123**, 3021–3036.

Prompers, J.J. and Brüschweiler, R. (2002) *J. Am. Chem. Soc.*, **124**, 4522–4534.

Radkiewicz, J.L. and Brooks, III, C.L. (2000) *J. Am. Chem. Soc.*, **122**, 225–231.

Ryckaert, J.P., Ciccotti, G. and Berendsen, H.J.C. (1977) *J. Comput. Phys.*, **23**, 327–341.

Schwarz, G. (1978) *Ann. Stat.*, **6**, 461–464.

Song, J. and Markley, J.L. (2003) *Biochemistry* , **42**, 5186–5194.

Tjandra, N., Feller, S.E., Pastor, R.W. and Bax, A. (1995) *J. Am. Chem. Soc.*, **117**, 12562–12566.

Tugarinov, V., Liang, Z., Shapiro, Y.E., Freed, J.H. and Meirovitch, E. (2001) *J. Am. Chem. Soc.*, **123**, 3055–3063.

Tugarinov, V., Shapiro, Y.E., Liang, Z., Freed, J.H. and Meirovitch, E. (2002) *J. Mol. Biol.*, **315**, 155–170.

Wallach, D.J. (1967) *J. Chem. Phys.*, **47**, 5258.

Wand, A.J. (2001) *Nat. Struct. Biol.*, **8**, 926–931.

Wax, M. and Ziskind, I. (1989) *IEEE Trans. Acoust., Speach, Signal Processing*, **37**, 1190–1196.

Woessner, D.E. (1962) *J. Chem. Phys.*, **3**, 647–654.

Wrabl, J.O., Shortle, D. and Woolf, T.B. (2000) *Proteins*, **38**, 123–133.

Yang, D. and Kay, L.E. (1996) *J. Mol. Biol.*, **263**, 369–382.

Ye, J., Mayer, K.L., Mayer, M.R. and Stone, M.J. (2001) *Biochemistry*, **40**, 7820–7831.